A Thorough Comparison Between Measurements and Predictions of the Amplitude Dependent Natural Frequencies and Damping of a Bolted Structure

Seyed Iman Zare Estakhraji[1], **Mitchell Wall**[2], **Jacob Capito**[3] **and Matthew S. Allen**[4],
[1]Post Doc., University of Wisconsin - Madison; zareestakhra@wisc.edu
[2]Graduate Student, University of Colorado-Boulder; Mitchell.Wall@colorado.edu
[3]Undergraduate Student, Brigham Young University
[4]Professor, Brigham Young University; matt.allen@byu.edu

ABSTRACT

Bolted joints are a significant source of damping and nonlinearity in built up structures. In the micro-slip regime (i.e. when the bolts do not slip completely) the log of the damping tends to increase linearly with the log of the vibration amplitude, the so-called power-law behavior. The natural frequency also tends to decrease slightly with vibration amplitude. While many works have successfully tuned phenomenological models to capture these behaviors, very few have sought to predict this behavior and none has predicted the nonlinearity in a bolted joint and validated the predictions with measurements over a range of bolt preloads and vibration amplitudes. This work presents a step towards such a prediction, using a detailed finite element model of a structure, including the preload forces in the bolts and Coulomb friction in the contact, to seek to predict the nonlinear damping and stiffness of the structure and how they vary with preload. The structure studied consists of two beams bolted together at their free ends, the so-called S4 Beam. While the contact interfaces were machined to be nominally flat, the micron-scale curvature in the contact interface is included in the model, approximated in two different ways, to seek to understand what fidelity is needed at the contact interface to successfully capture its dynamic behavior. The recently presented Quasi-Static Modal Analysis (QSMA) method is employed, where the amplitude dependent damping and natural frequency can be predicted from a single quasi-static simulation, avoiding the expense of numerical integration. The predicted damping and natural frequency are compared with measurements at various preloads, showing reasonable agreement if a Coulomb friction coefficient of 0.2 is used for all simulations. The simulations also revealed that, while the micron-scale curvature of the interfaces was important, the results were not very sensitive to how it was approximated.

Keywords: quasi static- Joints- damping- curvature- natural frequency

1. Introduction

For several decades, joints have been known to be a major source of damping [1], nonlinearity and uncertainty in structural dynamics. While many studies have sought to predict the behavior of joints, and some commercial software packages give the impression that this can be readily done, no study has ever presented a thorough prediction of the behavior of an actual joint and validated it with measurements. This challenge is relevant to many structures including blade-disk assemblies [2], [3], automotive brakes [4], bridges [5] and engines [6, 7]. Finite element modeling of structures has improved dramatically over the past few decades, and for monolithic structures one can accurately predict

ORCID(s):

their dynamic behavior and the resulting dynamic loads and/or stresses in a dynamic environment. However, almost all systems of practical interest contain joints such as bolts, rivets or welds. In the aerospace industry, the CAD geometry is typically simplified quite extensively (e.g. solids are replaced with shells, the actual geometry of joints is discarded and replaced with spiders and an approximate model such as a spring, dashpot, or a more advanced nonlinear element). Experimental measurements are then needed to validate or calibrate these elements and there is typically no attempt made at predicting the damping due to friction in the joints. Furthermore, joints often introduce nonlinearities into structures because of slip in the frictional contact at the interfaces. As the result, they are often sources of complicated phenomena such as of energy dissipation, stiffness loss, wear, modal coupling, response at higher harmonics, and even chaos [8, 9, 10, 11, 12]. While these effects certainly can be important, many aerospace structures have been successfully modeled as linear or quasi-linear. A quasi-linear system is a nonlinear system that is well approximated with a linear model in which properties such as the effective natural frequencies and damping ratios of some modes change with vibration amplitude [13, 12, 14].

It is important to be able to predict the effective stiffness and energy dissipation in a structure due to its joints. In many cases, the energy dissipated in the joints helps to reduce vibration amplitudes, and hence decreases stresses in a structure. In one study is was shown that the joints were responsible for 90 percent of the total system damping [15] and others have confirmed their importance [3, 10, 16, 17]. If one could more accurately estimate the energy dissipation due to the joints, one could leverage this to create more lightweight and efficient structures.

The interfaces between structures can exhibit many complicated and poorly understood phenomena, such as contact, friction, adhesion [18], [19], plastic flow and damage [20] and wear [9], and these can occur at a length scale that are several orders of magnitude smaller than that of the structure as a whole [21]. Even if one ignores many of those complications (as we shall do in this work) and considers only the mechanics of contact and stick/slip at the interface, the resulting models are still typically too expensive to simulate dynamically using numerical integration. To address this, Festjens et al. [22] proposed a method that decomposes the structure into two regions: a linear domain away from the joint, and a nonlinear domain near the joint, and then neglects the inertial term as the joint is assumed to behave quasi-statically. They then assumed that the structure would vibrate in a single mode of vibration and enforced the modal motion of the linear domain as a boundary condition on the joint region and were able to iterate to solve for the quasi-static response of the structure and from that they derived the effective natural frequency and damping ratio of the mode in question as a function of vibration amplitude. A variant on this method was developed concurrently by Allen et al. [23], who treated the entire structure and simply applied a static load that would excite only one mode of the linear structure and hence avoided iterating between the linear and nonlinear submodels. They dubbed their method "Quasi-Static Modal Analysis" or "QSMA" and successfully applied it to predict the response of reduced models where the joints were modeled as discrete Iwan elements [24]. They showed that QSMA was capable of giving very accurate

estimates of the amplitude-dependent modal damping and natural frequency in a tiny fraction of the time required by dynamic analysis. As the result, several researchers have been able to use QSMA to efficiently to tune reduced models to reproduce the nonlinear damping and nonlinear stiffness observed in experiments [24, 25, 26, 27, 28]. While these studies are encouraging, none addressed predictive modeling where the joint geometry, bolt preload force, and interface friction law are specified and used to predict the joint behavior from first principles.

In an effort to address this, Jewell et al. [29] applied QSMA to detailed FE models of a few structures with joints. They studied the mesh and solver settings needed to obtain acceptable predictions of the stiffness and damping of the joints, and presented the first comparison between simulation and experiment of the quasi-linear frequency and damping of the S4 Beam, a benchmark structure with two joints that was first studied by Singh et al. [30]. However, the study in [29] found that, to obtain agreement between the simulation and the experiments, the bolt preload had to be increased to twice the expected ultimate strength of the bolts. This suggested that more accurate modeling of the contact pressure in the joint was required. Brink et. al. [31] studied an S4 Beam with more carefully machined surfaces and modeled the contact in detail and verified their predictions using static pressure film in both the simulations and experiments. They successfully predicted the shift in the linear (i.e. low amplitude) resonance frequencies of the structure as the preload was increased. Following their lead, Wall et. al. [32] revisited the S4 Beam studied by Jewell et al. and showed that, while an FEA model with a flat interface (i.e. the nominal geometry) was not able to predict the linear natural frequencies, if the surface topology was included in the model then they could predict the shift in the linear natural frequencies versus preload.

This work builds on those efforts, seeking to understand the extent to which a finite element model can capture the linear and nonlinear behavior of the first six modes of the S4 Beam under a variety of bolt preloads. In doing so, we explore the fidelity with which imperfections in the interface topology must be captured in the model, and compare FEA predictions with measurements of both the linear natural frequencies and the quasi-linear natural frequency and damping versus amplitude of the two modes that exhibit the most nonlinearity. In previous studies the preload was found to be important and difficult to estimate from the bolt torque, so in the experiments shown here the preload in both bolts was measured with nominally identical load washers. The actual topology of the contact surfaces was measured using a coordinate measuring machine (CMM) and was smoothed using a locally weighted scatterplot smoothing method (Lowess) from Matlab® and then applied to a high fidelity Abaqus model. This was compared to a simpler approach, in which the surfaces were approximated with spheres and the radius of curvature is chosen to approximate the measured topology. In both cases, while the surface topology deviated from a perfectly flat surface by only about four to six microns (0.15 to 0.25 thousandths of an inch), those deviations caused clearly measurable changes to the linear natural frequencies. The experimental measurements presented here are also new, reflecting the latest experimental setup with two load washers and they were checked carefully against prior results to ensure that the vibration

amplitude was accurately reported and consistent between the measurements and the finite element models.

The comparisons reported here focus on two quantities. First, the linear natural frequencies of the first six modes predicted by the FE models are compared to measurements when very small inputs are applied to the structure. These linear natural frequencies are found to be sensitive to the preload, and so measurements are acquired at various preloads up to a level that approaches the ultimate strength of the bolts. This comparison informs the degree to which one can hope to use FEA to predict the natural frequencies of a structure with bolted interfaces. Second, the effective natural frequency and damping of two modes that exhibited the strongest nonlinearity were measured using high amplitude impacts and the results are compared to QSMA predictions from the FEM. If these quantities match, then one can be assured that the FEM can accurately reproduce the transient behavior of the beam at a range of forcing amplitudes.

The remainder of the paper is organized as follows: first the theory underlying QSMA is reviewed in Sec. 2 as well as the approach used by Abaqus to model frictional contact. The new experiments are summarized in Sec. 3, with the measurements and smoothing of the surface topology explained in Sec. 3.1 and 3.2 and the new dynamic measurements in Sec. 3.3. Finally, the comparison between the experiments and finite element predictions is presented in Section. 4.

2. Theoretical Background

2.1. Overview of QSMA

The quasi-static modal analysis method implemented in this paper is similar to one in [29, 33, 34], which is reviewed briefly here. The equation of motion of a structure with a joint is written as

$$\mathbf{M}\ddot{\mathbf{x}} + \mathbf{C}\dot{\mathbf{x}} + \mathbf{K}\mathbf{x} + \mathbf{f}_J(\mathbf{x}, \boldsymbol{\theta}) = \mathbf{f}_{ext}(t) \tag{1}$$

where $\mathbf{M}$ is the mass matrix, $\mathbf{C}$ is the damping matrix, and $\mathbf{K}$ is the stiffness matrix of the system, and $\mathbf{x}$, $\dot{\mathbf{x}}$ and $\ddot{\mathbf{x}}$ are the displacement, velocity, and acceleration vectors, respectively. The internal nonlinear force due to joints is represented by $\mathbf{f}_J$ and $\boldsymbol{\theta}$ is a vector containing the state of sliders (e.g. a Boolean to indicate whether each is currently stuck or sliding, if stuck the position at which each is stuck, etc...).

The first step is to preload the structure and solve a nonlinear quasi-static problem to obtain the preloaded state. In what follows we presume that this has already been done and that the displacements, $\mathbf{x}$, are displacements relative to the preloaded state. Then, at low amplitudes the joints can be treated as stuck and replaced with springs to create a matrix of joint stiffnesses, $\mathbf{K}_T = \frac{\mathrm{d}\mathbf{f}_J}{\mathrm{d}x}|_{x=0}$. The mass-normalized mode shape, $\boldsymbol{\varphi}_r$, of mode r can then be estimated by solving an eigenvalue problem,

$$([\mathbf{K} + \mathbf{K}_T] - \lambda_r \mathbf{M})\boldsymbol{\varphi}_r = 0 \tag{2}$$

where λ_r is the corresponding eigenvalue, which defines the natural frequency $\omega_r = \sqrt{\lambda_r}$. For the structures of interest, typically $\mathbf{C} = 0$ and material damping is used to define the damping ratio ζ_r of each mode. In this paper $\mathbf{C} = 0$ and the FE models report results without any material damping; material damping is removed from all experimental measurements so the only dissipation present should be from friction in the joints.

If we wish to understand the effect of friction on the rth mode of the structure, we apply a static force $\mathbf{f}_{ext} = \mathbf{M}\boldsymbol{\varphi}_r$. Doing so, only the mode r of system would respond if the structure were linear. This force is distributed over the structure and the resulting quasi-static nonlinear problem (to be solved by Abaqus) is

$$\mathbf{K}\mathbf{x} + \mathbf{f}_J(\mathbf{x}, \theta) = \mathbf{M}\boldsymbol{\varphi}_r \alpha_{\max} \tag{3}$$

where α is a scalar which sets the strength of the load. Eq. 3 is then solved in a FEA package to obtain $\mathbf{x}(\alpha)$ for N_α linearly spaced steps in the range $0 > \alpha \geq \alpha_{\max}$. The obtained results are mapped into the modal response of rth mode $q_r(\alpha) = \boldsymbol{\varphi}_r^{\mathrm{T}}\mathbf{M}\mathbf{x}(\alpha)$ and the modal force can be calculated as $\boldsymbol{\varphi}_r^{\mathrm{T}}\mathbf{M}\boldsymbol{\varphi}_r\alpha = \alpha$. As the result, $\mathbf{x}(\alpha)$ and α define the backbone part of the hysteresis curve of the system. Masing's rule can then be applied to find the loading and unloading parts of the hysteresis curve [22, 29]. The instantaneous natural frequency of the mode is then calculated using the secant of the hysteresis curve

$$\omega_r = \sqrt{\frac{\alpha}{q_r(\alpha)}} \tag{4}$$

Moreover, the area under the hysteresis curve, $D(\alpha)$, is used to find the energy dissipation $D(\alpha)$, and the effective damping ratio is calculated as

$$\zeta_r = \frac{D(\alpha)}{2\pi(q_r(\alpha)\omega_r(\alpha))^2} \tag{5}$$

The QSMA procedure was performed in Abaqus by implementing a three-step analysis, first the preload was applied on the model to bring the surfaces to contact, then the linear modal analysis was performed to obtain mode shapes and natural frequencies of the system. Please note that for the linear modal analysis, Abaqus considers the nodes that are in contact to be tied together. Finally the nonlinear quasi-static step is implemented where Abaqus solves the nonlinear equation explained in Eq. 3. An overview on this implementation is explained here, however, for more detail please refer to [29].

In implementing the steps described above, the dissipated energy was calculated using the trapezoidal rule on the force-displacement curve. The procedure was typically applied to the first five samples of the force-displacement curve, using Eq. 4 and Eq. 5 to compute the effective frequency and damping at that displacement amplitude. The

process was then repeated for the first six points and so on until all N_α points on the loading curve had been used. Typically $N_\alpha = 50$ in the results reported here. As a result, the damping ratio and natural frequency are found as a function of displacement amplitude $q_r(\alpha)$. In order to report the results in physical units, the peak modal displacement for each load step was calculated by multiplying the modal displacement by the mode shape at the point where the deflection is largest. The peak displacement was then used to estimate the peak velocity by assuming that the response is quasi-linear so that $v_{peak} = x_{peak}\omega_r\sqrt{1-\zeta_r^2}$.

2.2. Solving the Nonlinear Contact Problem in Abaqus

In this paper, the S4 beam is modeled in Abaqus/Standard [35]. Abaqus/Standard provides several contact formulations, which depend on the contact discretization and tracking approaches chosen by user. In all cases presented in this paper the "finite-sliding" tracking approach was chosen, as no speedup was observed if "small-sliding" was employed instead, and the latter approach becomes inaccurate if the slip is too large.

Moreover, Abaqus/standard simulates contact conditions by applying the constraints at various locations based on the discretization method chosen for the problem. There are two main discretization methods for the contact surfaces in Abaqus: the Node-to-Surface (N-S) and the Surface-to-Surface (S-S) methods. In the N-S method, each slave node interacts with a point of projection on the “master” surface. The penetrations of slave nodes into the master surface are simply resisted resulting in spikes and valleys in the stress/pressure distribution. However, in S-S method the contact conditions are enforced in an average sense over regions including nearby slave nodes. In this method, each contact constraint considers a finite region of the slave surface. Therefore, although some penetration may be observed at some nodes, large penetration of the master nodes into the slave surface is prevented. The S-S method was employed in this work; the other approaches were not attempted.

In order to enforce contact and friction, the penalty method was used in this paper in both the normal and tangential directions. The penalty method in the tangential direction was explored and discussed in some detail in [29]. To explain the concept briefly, consider the normal direction. It is typically extremely difficult for the solver to find a solution in which the nodes of the two contacting surfaces have precisely the same displacement (or zero relative displacement). Hence, the penetration is defined as the relative displacement of the two surfaces, $p(u)$ in Fig. 1 and used to drive the solution towards the desired solution in which the penetration is zero. If the penetration is negative then no force is applied between the nodes, whereas if it is positive then the solver applies a force to the penetrating node that is proportional to the penetration. The constant of proportionality is the contact stiffness. In Abaqus, the representative underlying element stiffness is chosen as the default initial penalty stiffness [35], and one could increase it to obtain a solution that is closer to a Lagrange contact simulation. One the other hand, rough surfaces have a finite contact stiffness that arises due to deformation of the asperities at the surface. This can be measured [36, 37] and used to

calculate a penalty stiffness that is physically meaningful. However, the surfaces of the S4 Beam that are studied in this work are highly polished and so it didn't seem prudent to reduce the penalty stiffness. In this paper, Abaqus's default setting is used in order to drive the solution towards a Lagrange solution; in a subset of the simulations this was increased by as much as 50 times and found to have a negligible effect.

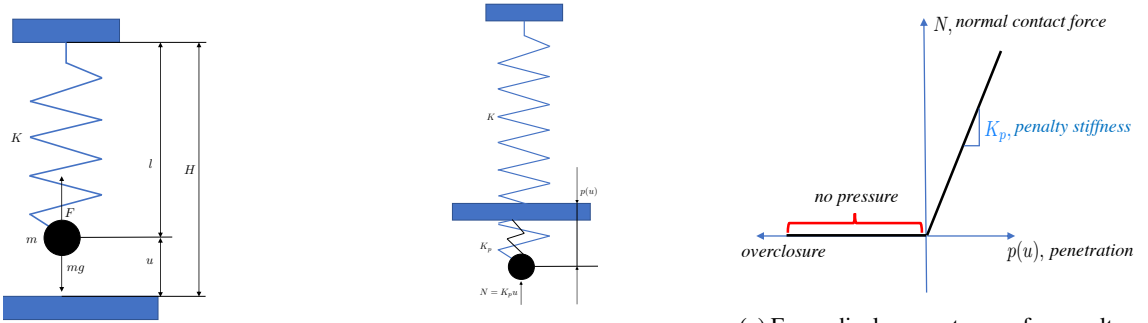

(a) Spring-mass system

(b) Spring-mass system in contact with a rigid plane with penalty method

(c) Force-displacement curve for penalty method

Figure 1

3. Experiments

As mentioned previously, the structure studied in this work is the S4 Beam [30], which consists of two prismatic beams bolted together at their ends. Each beam is 20 in (508 mm) long, 1.25 in (31.75 mm) wide and 0.38 in (9.652 mm) thick, except that the last 2.0 in (50.8 mm) of each beam is 0.50 in (12.7 mm) thick, so that contact only occurs over this region. Further details and finite element models of the structures are available at the website mentioned in [32].

3.1. Surface Measurements

The contact interfaces of B5B6 beams were machined to be nominally flat, and so they were modeled as flat in our prior work [29], and yet that model could not capture the physics observed in the S4 Beams, and so the surface topology of the experimental structures were measured in detail in order to increase the fidelity of the finite element models. These measurements were used in two ways: 1.) They were used to estimate an effective radius of curvature of the surface, which was then applied to the FEM and 2.) They were smoothed and applied to the FEM directly

The topology at the contacting surfaces was measured using G2 Contoura coordinate measuring machine (CMM) with a manufacturer stated accuracy of 79μin (2 μm). A grid of roughly 11, 000 points was measured on each interface. During the measurement, the beam was bolted flat onto the measurement table, and an epoxy plug was used to fill the bolt hole so the machine could easily cover the whole surface in a single measurement. Note that in the raw measurements from the CMM, the left and right surfaces had slightly different heights and the surface showed a nonzero

slope. It was judged that these features would not be accurate for the instrument used. Furthermore, simulations revealed that one need only apply a small fraction of the preload to bring the surfaces into alignment, and so the mean and slope of the measured data was removed prior to any further analysis. The measurements for B5B6 are shown in Fig. 2. It can be seen that the two sides of each beam, i.e. Fig. 2a and Fig. 2b or Fig. 2c and Fig. 2d, have different surface topology and none is exactly flat. The difference in height between the corners of the contact patch and the area near the bolt ranges from about 0.15 to 0.25 mil (3.8 to 6.4 μm) over the four surfaces.

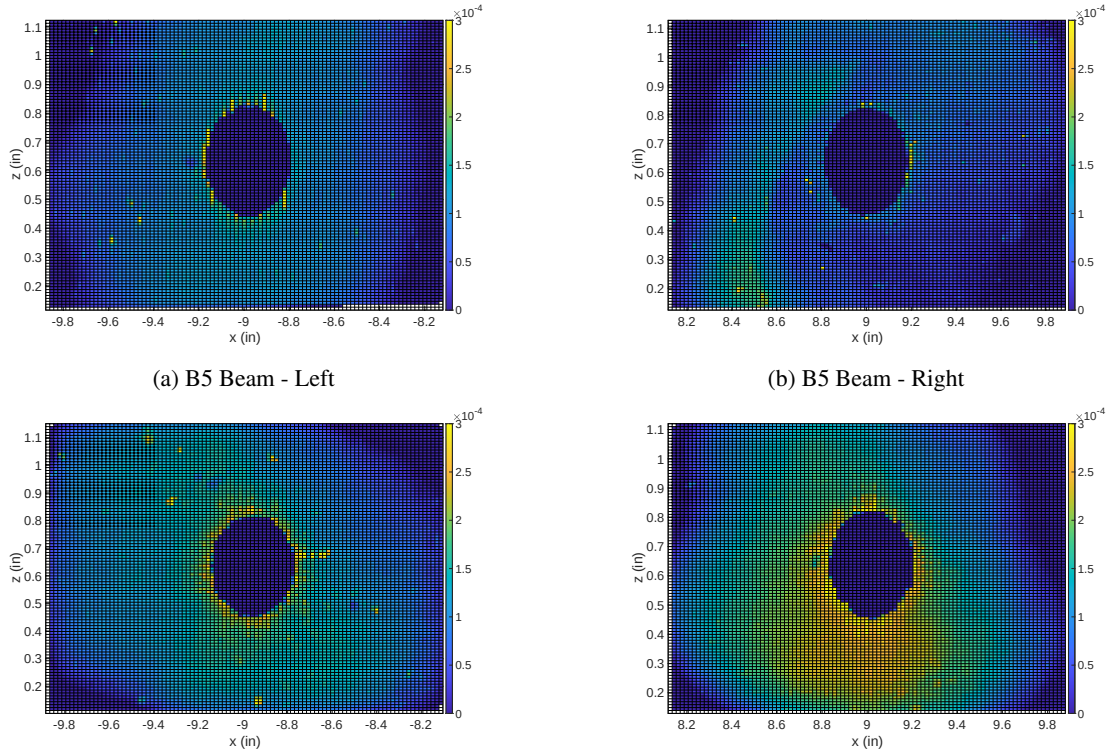

(a) B5 Beam - Left

(b) B5 Beam - Right

(c) B6 Beam - Left

(d) B6 Beam - Right

Figure 2: The surface topology of the four surfaces measured, two on each end of the beam. The color bars are in inches.

To approximate these surfaces as spherical, a spherical surface was found that best matched the height differences observed in Fig. 2. Specifically, to capture the 0.15 to 0.25 mil (3.81 to 6.35 μm) height differences over the 2 in by 1.25 in (50.8 mm by 31.75 mm) patches, a radius of curvature of 4.6e3 and 2.8e3 in (1.17e5 and 7.11e4 mm) would be needed. For simplicity, spherical surfaces with R=1000, 2000, 4000 and 8000 in were created. To evaluate the ability of the models to capture the actual surface topology, the unsmoothed surface topology was applied to the FEM and two-dimensional slices along the contact surface at two different locations are plotted in Fig. 3. These are compared to the topology of the models that had spherical curvature. (Similar results are also shown for the surfaces that were smoothed with the lowess method, as described in the next subsection.) Note that in each case the surfaces were

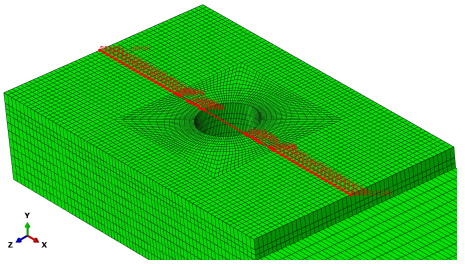

(a) Slice at z=0.65 in (16.51 mm)

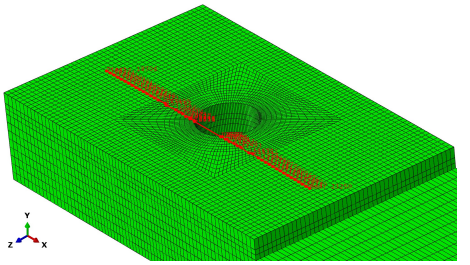

(b) Slice at z=0.75 in (19.05 mm)

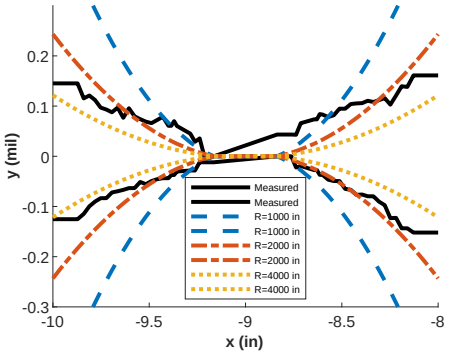

(c) Sphere Profiles at z=0.65 in (16.51 mm)

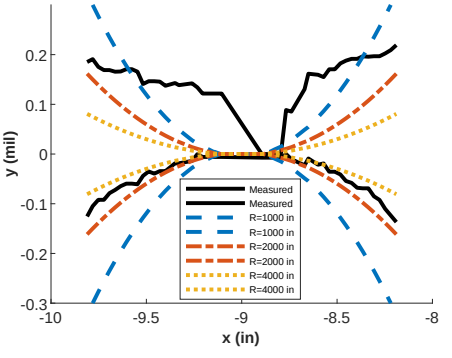

(d) Sphere Profiles at z=0.75 in (19.05 mm)

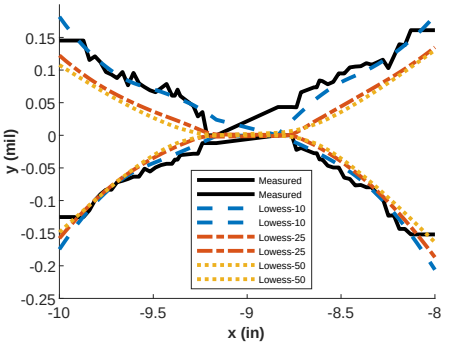

(e) Lowess Profiles at z=0.65 in (16.51 mm)

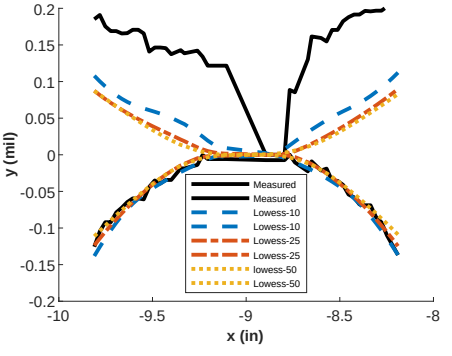

(f) Lowess Profiles at z=0.75 in (19.05 mm)

Figure 3: Two-dimensional slices of the surfaces from different models at two paths $z = 0.65$in (16.51 mm) and $z = 0.75$in (19.05 mm)

translated in the y-direction so that a single pair of nodes was initially in contact.

It should be noted that it would not be highly accurate to approximate any of the measured surfaces as spherical, but such an approach would probably be much more tractable in industrial applications if it gives reasonable results. Based on the slices shown in Fig. 3, the best model would likely have R=3000 in (7.62e4), midway between the R=2000 in (5.08e4 mm) and R=4000 in (1.016e5 mm) models that were created.

3.2. Surface Smoothing

As mentioned previously, the second approach used in this paper was to apply the surface measurements directly to the FEM. However, it was necessary to apply some smoothing first otherwise the contact would happen at a few discrete nodes. The measured surface data was smoothed using a locally weighted smoothing method [38, 39], which is called the "Lowess" method in the "fit" function in Matlab. Using this approach, each data point is replaced with its fitted/smoothed value, using a local polynomial weighted least squares regression. Only the neighboring data points are used to determine the smoothed value for each data point; specifically one defines a percentage p of the data to use and that percent of the nearest neighbors are used in the computation. Each data point contained within the span is also weighted by the regression weight function in Eq. 6,

$$w_i = \left(1 - \left|\frac{x - x_i}{d(x)}\right|^3\right)^3 \tag{6}$$

where x_i are the nearest neighbors of the point of interest, x. Defined by the span p, x is the predictor value associated with the response value to be smoothed and $d(x)$ is the distance from x to the most distant predictor value. Note that the data point desired to be smoothed has the most influence on the fit. After determining the weights for each data point, a weighted linear least-squares regression (linear polynomial) is performed.

In this paper, to vary the degree of smoothing applied, different span values were applied, and each is reported as "Lowess-p", i.e. "Lowess-10" uses 10% of the nearest neighbors in the smoothing. Because our measurements were approximately uniformly distributed over the surface, a smoothing factor of 10% would correspond to data within about a 0.2 in (5.08 mm) radius of each point. Two-dimensional slices of the surfaces, smoothed with the lowess method with $p = 10$, 25 and 50 percent are shown in Fig. 3. One can observe that lowess-10 still retains some of the jaggedness of the surface, while the other two give similar results and result in quite smooth surfaces. As a further illustration, the three-dimensional surface profiles after smoothing with Lowess-50 are shown in Fig. 4.

Once the smoothed surfaces had been created, they were used to compute the height of the nodes of the FEM over the contacting surfaces (i.e. the raised regions in the S4 Beam). The in plane coordinates (x, z) were used to compute the height of the smoothed surface, and the nodes in the FE model were moved up slightly to have the desired surface height. The displacements required to accomplish this were small (less than 0.001 in or 25 μm) relative to the size of the mesh (0.025 or .635 mm) and so any mesh distortion was negligible. As an example, the lowess-50 smoothed topology in Fig. 4 was applied to the FE mesh and the initial positions of the contacting nodes are visualized in Fig. 5.

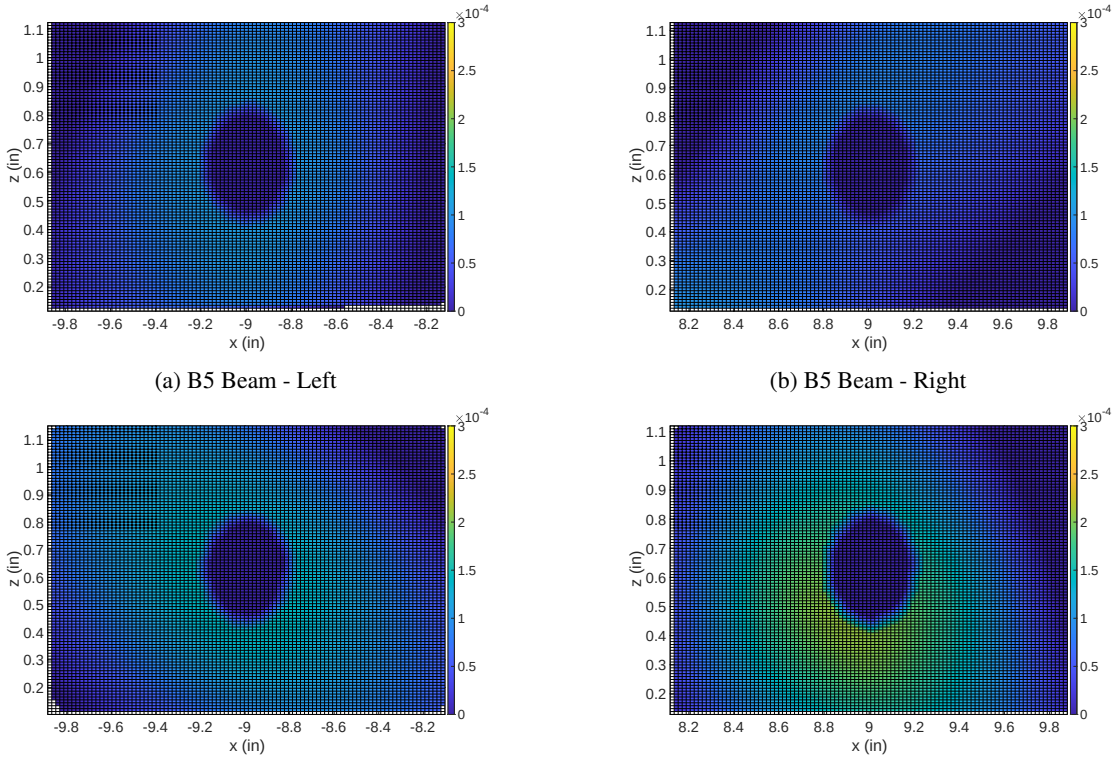

(a) B5 Beam - Left

(b) B5 Beam - Right

(c) B6 Beam - Left

(d) B6 Beam - Right

Figure 4: The profiles of fitted surfaces for B5B6 using Lowess-50. The color bars give the height of the surface in inches.

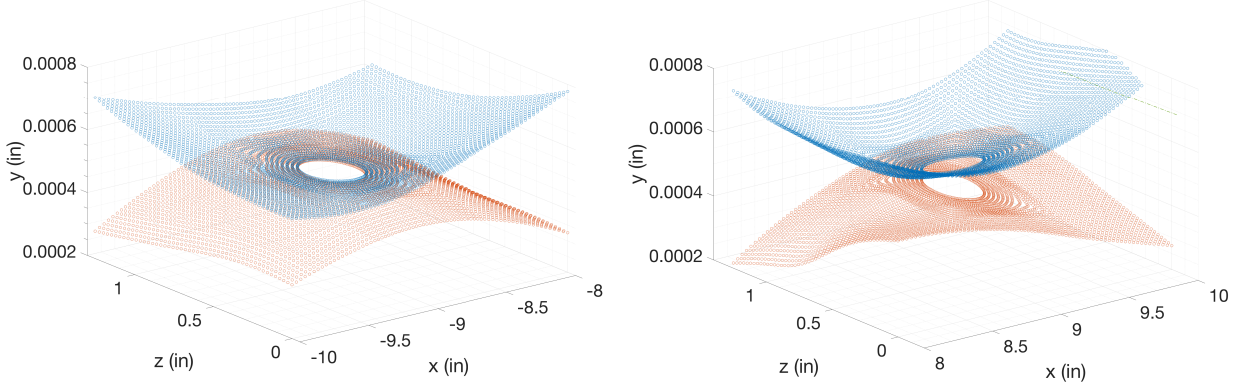

(a) B5B6 Beam - Left

(b) B5B6 Beam - Right

Figure 5: Contact surfaces of the left and right sides of the FEM when the lowess-50 topologies, shown in Fig. 4, are applied. a) The surfaces for the left side of the beam from Fig. 4a and Fig. 4c, b)The surfaces for the right side of the beam from Fig. 4b and Fig. 4d

3.3. Dynamic Measurements

Experiments were conducted to estimate the linear natural frequency of the structure (e.g. for small amplitudes) as well as the natural frequency and damping as a function of vibration amplitude. The structure tested here is identical to the "2017 Beam" tested in [32], with the specific pair of beams used called B5 and B6 in prior works. However, the structure tested here had two load cells, one on each bolt, to ensure that both bolts had the same preload. (The torque applied to each bolt was increased carefully until the load cells indicated the desired preload.) The S4 beam was suspended with bungee cords to approximate free-free boundary conditions, as shown in Fig. 6. Six accelerometers were used so that the fundamental modes could be distinguished using a modal filter. The accelerometers were at the following nodes: [B100Z,B200Y,N200Y,B200-Z,B250Z,B300Z] with 100 denoting the left side of the beam and 300 the right side, B denoting the beam on the bolt side and N denoting the beam on the nut side (the back), and the directions as shown in Fig. 6. Additional details on the test setup can be found in [32].

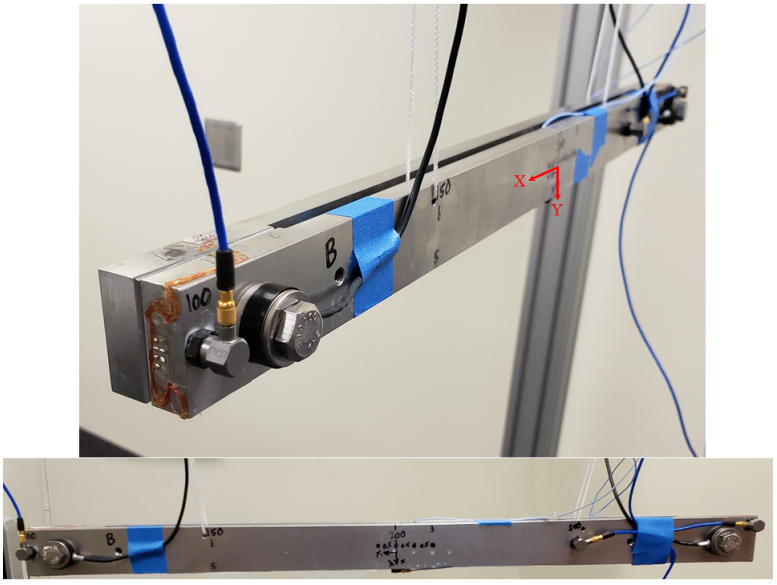

Figure 6: Photo of the experimental setup used when testing the S4 Beam.

The tests for the beams consisted of three steps. The beam was first excited at low level with a very light impact hammer (with peak forces $<$ 1N) to extract the linear natural frequencies, damping ratios and mode shapes of the structure. Then, several high amplitude impacts (50N - 700N) were applied with a large hammer to excite nonlinearity in the modes of interest. These tests were used to assess the damping and frequency as a function of amplitude. Finally, the linear test was repeated to check whether the linear properties had changed significantly (i.e. if a bolt slipped). Frequency response functions were measured in the linear tests and the Algorithm of Mode Isolation [40]. For the nonlinear tests, the time histories of the response were measured, modally filtered using the mode shapes extracted from the linear test, and used to calculate the frequency and damping as a function of amplitude using the

Hilbert transform [41]. See [32] and [42] for further details on the post-processing of the measurements.

When performing the tests reported in this paper, specific attention was given to the scaling of the measurements. Specifically, in prior works the mass normalized mode shape was extracted from the measurements and used to scale the horizontal axis in figures such as Fig. 11. Some inconsistencies were found in prior works, specifically in the scale used in [29], causing the damping to be significantly under-estimated at a given amplitude in [29], and so the procedure was checked carefully. Additionally, the mass normalized mode shapes found experimentally were compared with those found by the finite element model and found to agree within a few percent, lending additional confidence to the experimental procedure. In the end, to ensure consistency between the experimental measurements, Mode 2 was always scaled such that its mass normalized mode shape at the measurement point B200Z was 0.914 $kg^{-1/2}$ and Mode 6 was always scaled to a value of 0.842 $kg^{-1/2}$ at point N200Y.

4. Results

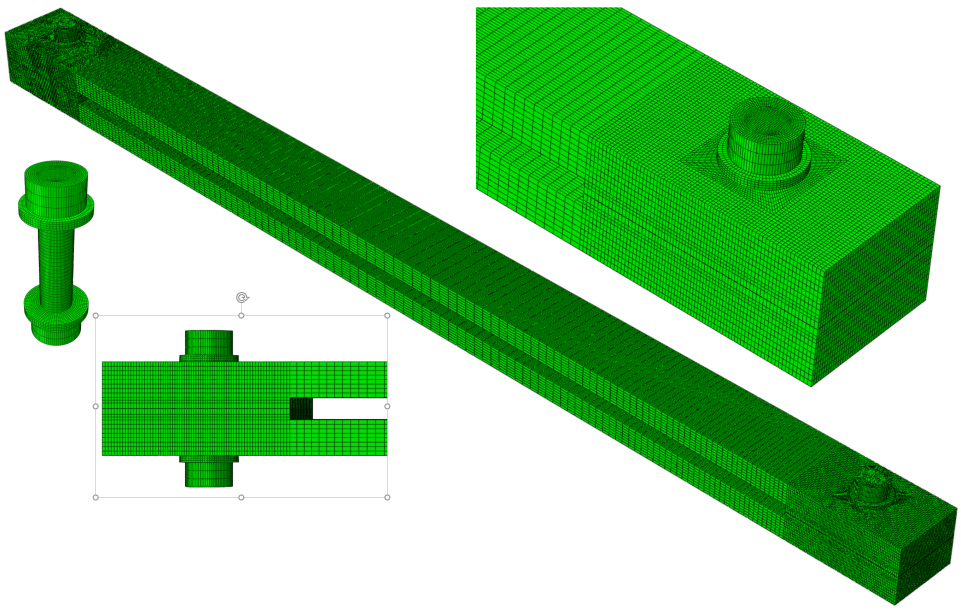

Figure 7: Finite Element Mesh used for the S4 Beam.

The finite element model used in this work is shown in Fig. 7. The model consisted of 387,114 nodes (1.16M degrees of freedom), with 341,504 elements of the type C3D8 and C3D8R in Abaqus. The reduced integration (C3D8R) elements gave erroneous contact pressures when used near the contact, so they were only used for the portions of the beam away from the contact in order to minimize shear locking in this region when the beam bends. The bolts, nuts and washers were approximated with cylinders as shown. The load washers seen in Fig. 6 were unfortunately not included, as they were added to the experimental setup after all of the analysis had been completed. The side view on

the bottom right shows the contact interface, where the surface profiles were applied. The model shown is for R=2000 in, although the curvature and gap between the elements is not visible at this scale.

4.1. Linear Frequency Study

The first metric used to evaluate the performance of the finite element models was their ability to predict the natural frequencies of the assembly. When two flat surfaces some into contact, the contact area is independent of the clamping force [43], and hence the stiffness of the contact is also independent of the preload. This was confirmed for the FE models of the S4 Beam in [32], where a model with flat contact interfaces was found to predict natural frequencies that were independent of the preload. In contrast, when curved surfaces come into contact (as can be seen in Hertzian contact), the preload changes the contact area and hence the stiffness of the contact. As will be shown below, the experimentally measured natural frequencies for the S4 Beam showed this same behavior, confirming the importance of the interface curvature if one is to model the structure accurately.

Before presenting the frequencies, it is informative to see how the contact pressure at the interface changes as the surface topology changes. Figure 8 shows the contact pressure for the nominal model with a perfectly flat interface and that for four models with Lowess smoothing. The contact pressure can be seen to change very significantly, and this causes the effective contact area to change, leading to the changes in the natural frequencies observed below.

Table 1 shows the linear natural frequencies of the first six modes as measured on the S4 Beam when the preload in each bolt was 2000 lb. The measurements were repeated on two different days, once before applying high amplitude impacts and once after, for a total of four measurements. The values in parenthesis are the standard deviations (in Hz) of the measurements for each mode. The natural frequencies predicted by each of the finite element models are also shown. For reference, the mode shapes of these modes are shown in Fig. 9 for the nominal model. The mode shapes of all other FEMs reported in the paper were visually indistinguishable at this scale; the changes in the shapes were small and localized to near the contact interface. Note that, prior to these predictions, the density of the steel in each finite element model was adjusted so that the mass of the FEM matched that of the measured mass of the actual S4 Beam, and the elastic modulus was updated so that the FEM predicted the natural frequencies measured on a single beam (i.e. half of the assembly with no joints) as well as possible. The final values were $\rho = 0.2894$ lb/in^3 and $E = 28.14 \times 10^6$ psi, and these brought the natural frequencies into agreement within 1% on average.

The natural frequencies predicted by the models are all in good agreement with those measured experimentally. Mode 4's natural frequency is nearly independent of the model, because it induces almost no stress on the joint, and similarly for Mode 3. Modes 1, 2 and 6 are most sensitive to the joints and show varying levels of agreement as the curvature in the model changes.

The natural frequencies were also measured and computed at preloads of 500, 1000 and 1500 lb, and the changes

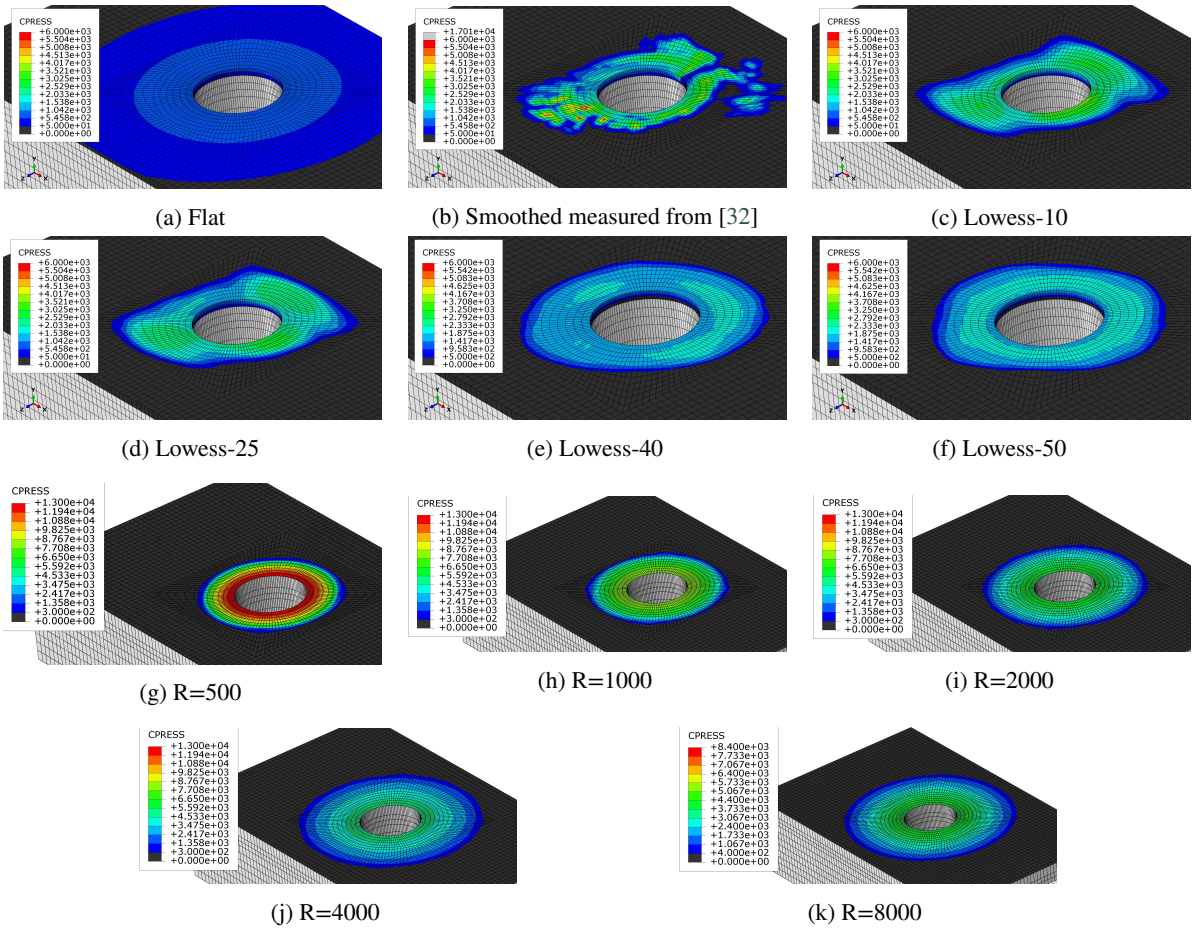

(a) Flat (b) Smoothed measured from [32] (c) Lowess-10

(d) Lowess-25 (e) Lowess-40 (f) Lowess-50

(g) R=500 (h) R=1000 (i) R=2000

(j) R=4000 (k) R=8000

Figure 8: The contact pressure distribution of the left side of the beams for various interface shapes. Figures(a)-(f) are for 500 lbs preload and (g)-(k) are for 2000 lbs

Case	Mode 1	Mode 2	Mode 3	Mode 4	Mode 5	Mode 6
Experiment	262.58 (0.18)	331.26 (0.06)	476.91 (0.08)	565.16 (0.08)	718.34 (0.59)	860.21 (0.72)
R=1000	253.72	328.26	478.93	566.68	690.33	796.27
R=2000	256.94	329.21	478.96	566.65	700.06	821.65
R=4000	260.5	330.56	479.01	566.64	710.91	849.76
Lowess-10	259.66	330.38	479.01	566.65	708.45	848.21
Lowess-25	258.92	330.01	478.99	566.65	706.14	839.57
Lowess-50	259.07	329.97	478.99	566.64	706.54	838.34

Table 1: Linear natural frequencies (Hz) for 2000 lb preload. The standard deviation of the experimental measurements is shown in parenthesis.

in the natural frequencies relative to the 2000 lb preload state were computed and are plotted in Fig. 10. By computing the frequency shift, any offset between the models due to inaccuracies in the modulus, density or mesh is eliminated and one can evaluate the ability of the models to predict the effect of the preload.

The largest frequency shifts occur for Mode 1 (opening and closing mode) and Mode 6 (torsion). The FEMs with spherical curvature with R=2000 or 4000 reproduce the behavior of these modes the best at the 500-lb preload, and

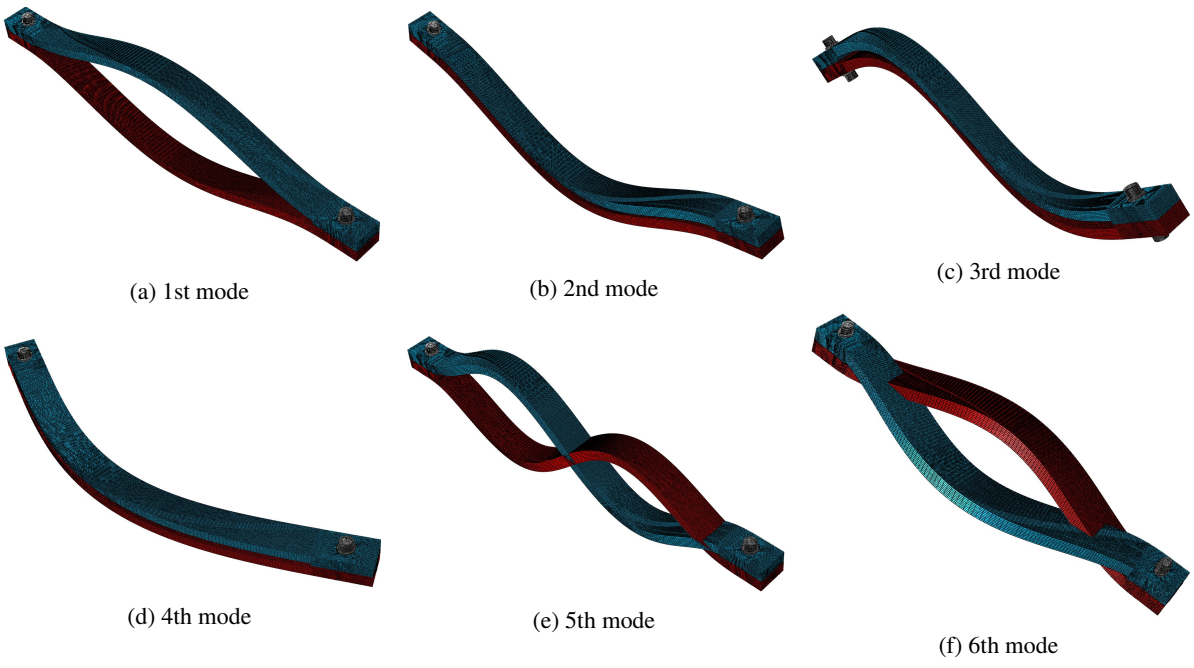

(a) 1st mode (b) 2nd mode (c) 3rd mode

(d) 4th mode (e) 5th mode (f) 6th mode

Figure 9: Mode shapes for the nominal the S4 beam FEM.

are reasonably close at the higher preloads. The FEMs with the actual surface topology smoothed with lowess-25 and lowess-50 give the best results among those models, although their performance is not dramatically better than the models that approximated the surfaces as spherical. Mode 2 (symmetric bending) has a smaller frequency shift, but as will be seen subsequently, this mode has highly nonlinear damping due to the joint and hence it is of particular interest. Once again, both types of models seem to predict its behavior well, perhaps with a preference for the lowess-10 model at 500 lb preload.

4.2. Nonlinear Behavior

While Modes 1, 2 and 6 were all found to be significantly affected by the joints, Mode 1 exhibits an opening-closing nonlinearity that affects its natural frequency but not its damping. This work is focused on understanding the damping dominated nonlinearities exhibited by bolted joints, and so no further attention was paid to Mode 1.

Quasi-static modal analysis was applied to several of the models to compute the effective amplitude dependent natural frequency and damping ratio of Modes 2 and 6. Prior works have shown that these should be comparable to the experimentally measured frequency and damping when one mode is excited in isolation [44], and our previous study [32] identified the drive points for which this was true for the S4 Beam. Each analysis took a few days to complete on a modern desktop computer (Intel Pentium Quad-core i7 at 3.6 GHz with 32MB RAM) using between 2-4 cores, or on the University of Wisconsin's Center for High Throughput Computing cluster. In order to thoroughly study the effect of surface shape, friction coefficient and other parameters on the results, more than 50 analyses were completed totaling

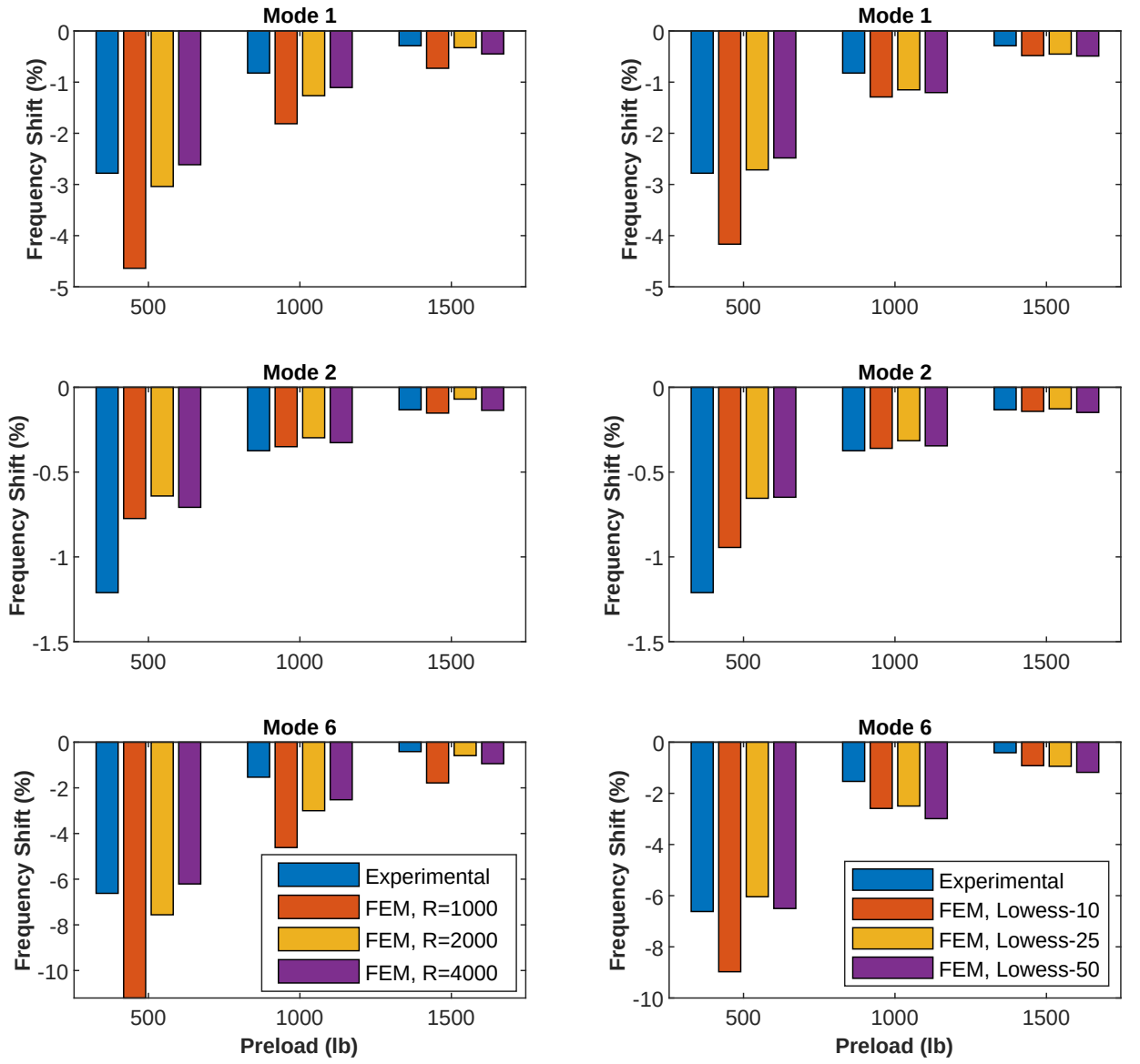

Figure 10: Percent change in the natural frequencies relative to 2000 lb preload case for experimental measurements and various finite element models. FEMs with spherical curvature (left), and FEMs with the measured topology, smoothed using the lowess method (right).

thousands of CPU hours. Several models failed to converge for certain preload levels, some even after considerable effort adjusting the convergence tolerances and contact settings. The subsections below present the results for the two extreme values of preload: 500 lb and 2000 lb for many of the finite element models with spherical and smoothed surfaces.

4.2.1. Mode 2 with 500 lb (2220 N) Preload

Prior to presenting the results in detail, some comments are in order regarding the results and post processing. Figure 11 shows the measured damping ratio of Mode 2 as a function of vibration amplitude, as well as QSMA predictions from various models with the same 500 lb (2220 N) preload. The vibration amplitude is expressed in terms of the peak velocity. Specifically, when the structure vibrates in Mode 2, the largest displacement or velocity or acceleration is obtained at a node at the center of the S4 Beam in the $y-$ direction. The horizontal axis in all of these figures corresponds to that velocity. Because the response is quasi-linear, one could convert this velocity, whose peak value is 2.0 in/s (50.8 mm/s) in Fig. 11, to a displacement by multiplying by the instantaneous natural frequency, which is approximately 328 Hz for all of these models, see Table 1 and Fig. 10. Hence, the peak displacements in the measurements in Fig. 11 would be 9.7×10^{-4} in or $25\mu m$, and the peak acceleration would be 10.7 g. The same approach will be used for the torsional Mode 6 in subsequent results, only its peak displacement occurs in the $z-$ direction.

When comparing the QSMA results to measurements, some anomalies were often observed, as indicated with arrows in Fig. 11. Starting at high amplitudes, the predicted damping curves show power-law behavior [45], or a situation in which the log of the damping increases linearly with the log of the vibration amplitude. However, at low enough vibration amplitudes (corresponding to low enough forces or displacements in the quasi-static analyses), the models often showed a deviation from this behavior; in the cases in Fig. 11, the damping increases above the power-law trend. This was investigated and the reason seems to be that, when the displacement is small enough for a given mesh, the number of elements sticking or slipping does not change from one load increment to the next, and hence any estimate of damping is dominated by artificial damping or compliance in the interface and not due to friction. There is always a finite compliance in these interfaces because the penalty method is used to enforce the contact. This is illustrated in Fig. 12, which shows the element faces that were open, in contact and stuck and slipping at various points along the quasi-static solution for the spherical interface model with $R = 2000$. As the displacement doubles the contact evolves noticeably for points in the power-law regime (i.e. for velocities above 2.0 in/s), while there is no significant slip at lower velocities (i.e. lower quasi-static displacements). The effect of the slight curvature on the interface can be seen by comparing Fig. 12 with the corresponding result in [29], which was created for the beam with a flat interface.

In light of these observations, the only valid part of the QSMA curves is that for which significant slip does occur. Hence, results for smaller displacements can be discarded. Figure 13 shows the same result but with the spurious regions removed. The corresponding frequency versus amplitude behavior is also shown. In the remainder of this paper, only those portions of QSMA predictions that were thought to be physically meaningful are shown.

One question that often arises with regard to bolted joints is whether one must account for variations in the contact

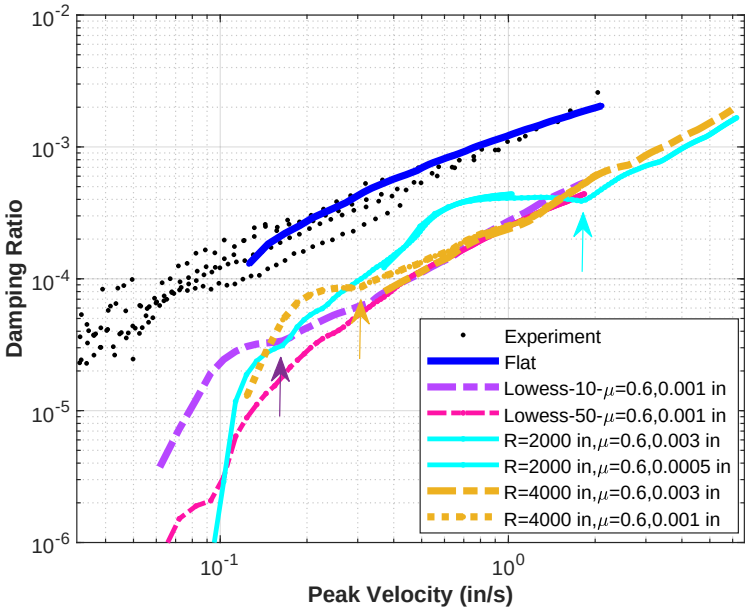

Figure 11: Sample results for Mode 2 at the 500-lb preload for $\mu = 0.6$ for various force levels α and models with different surface profiles (i.e. Lowess-10 and -50 smoothed surface profiles or surfaces with spherical curvature with $R = 2000$ and $R = 4000$).

pressure as the structure vibrates. For example, for the Brake-Reuss beam studied in [46], the contact pressure was observed to vary considerably. This was investigated in the simulations performed here, and in all cases the contact pressure was found to be essentially constant as the quasi-static load (i.e. the modal vibration amplitude) increased. For example, for the model with $R = 2000$, 500 lb preload, $\mu = 0.6$, the contact pressure varied by only 0.1% over the range of quasi-static loadings shown in Fig. 11. If this was not the case, then one could perhaps use the extension to Masing's rules presented in [47].

After eliminating the spurious computational results, one can see in Fig. 13 that there are considerable discrepancies between the measured frequency and damping and that predicted from the FEM. The model with a flat interface (the nominal geometry) predicts the damping very accurately and shows fairly accurate frequency behavior, although the frequency decreases too quickly with increasing response amplitude. However, in Sec. 4.1 we mentioned that this model is completely incapable of predicting the effect of preload on the natural frequencies of the various modes. The other models all show damping that is about an order of magnitude too small and have the frequency shift occurring at too large of amplitudes. Interestingly, the models are all surprisingly consistent in their predictions of the frequency and damping. This suggests that one may only need an approximation of the surface geometry to accurately predict the nonlinearity; even though there were significant differences between how the interface was approximated by the Lowess 10 and 50 models or the R=2000 and R=4000 in models, all of these models predicted about the same nonlinear behavior.

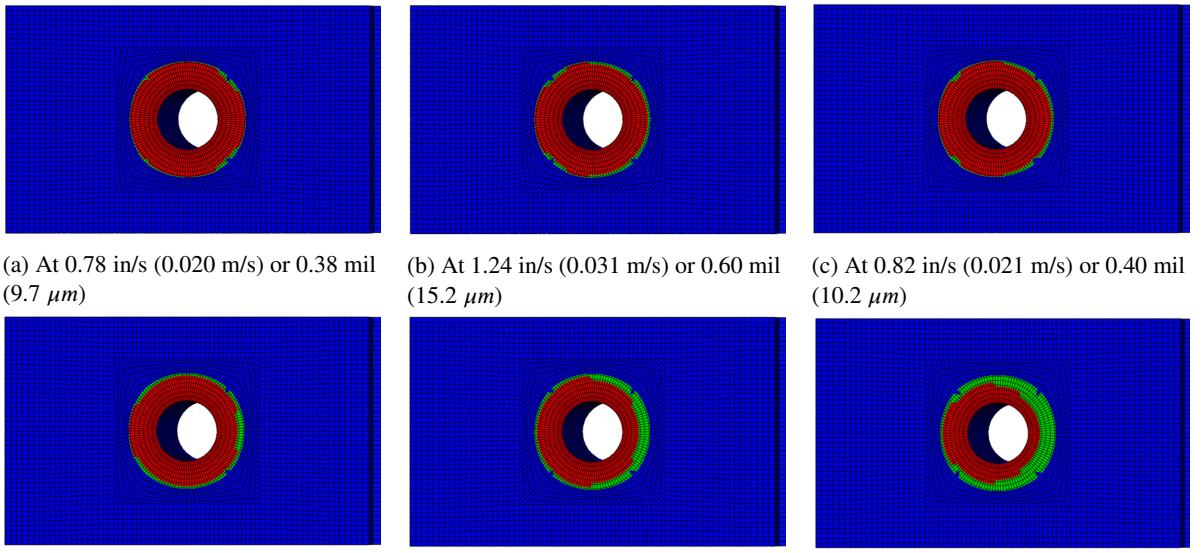

(a) At 0.78 in/s (0.020 m/s) or 0.38 mil (9.7 μm)

(b) At 1.24 in/s (0.031 m/s) or 0.60 mil (15.2 μm)

(c) At 0.82 in/s (0.021 m/s) or 0.40 mil (10.2 μm)

(d) At 1.90 in/s (0.048 m/s) or 0.92 mil (23.4 μm)

(e) At 3.83 in/s (0.097 m/s) or 1.86 mil (47.2 μm)

(f) At 6.43 in/s (0.163 m/s) or 3.12 mil (79.3 μm)

Figure 12: Contact status over the 1.25 by 2 inch contact patch for the spherical interface model, $R = 2000$, 500 lb preload, $\mu = 0.6$, at various displacement levels of Mode 2: (blue) not in contact (red) stuck (green) in contact and slipping.

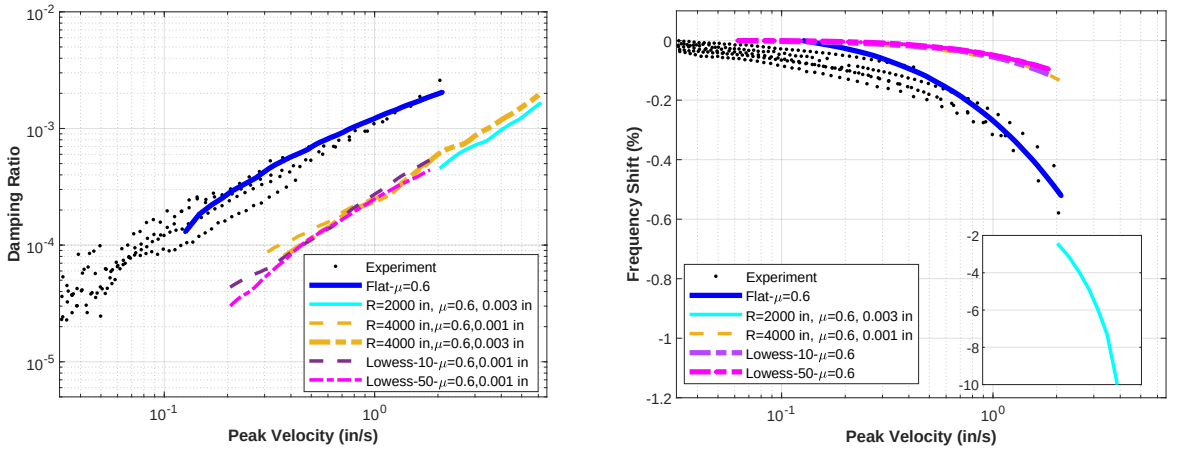

Figure 13: Frequency and damping versus amplitude for Mode 2 at the 500 lb (2220 N) preload for $\mu = 0.6$ for various force levels α and models with different surface profiles (i.e. Lowess-10 and -50 smoothed surface profiles or surfaces with spherical curvature with $R = 2000$ and $R = 4000$) after removing the spurious part of each curve.

All of the results presented so far assumed a friction coefficient of $\mu = 0.6$, which was based on tests performed on rigs such as those in [48]. (The static and dynamic or sliding coefficients of friction were assumed to be equal.) A smaller coefficient of friction might be justified if one considers that a friction coefficient of $\mu = 0.6$ is typical for stainless steel surfaces after a break in period where the oxide layer is worn away. Stainless steel contacts are reported to have smaller coefficients of friction, i.e. $\mu = 0.2 - 0.3$ prior to this break in period. It is unclear which friction mechanism might dominate in these joints, where microslip is the dominant mechanism. Additional simulations were run with smaller coefficients of friction to see if this would increase the slip and damping and bring the results into better correspondence.

Figure 14 shows the results of these simulations, compared to the same experimental data that was described previously. The results show that reducing the friction coefficient from $\mu = 0.6$ to $\mu = 0.2$ brings the QSMA predictions into much better agreement with the measurements, although the damping is still under-predicted by about a factor of two and the frequency shift still occurs at too large of amplitudes. Further decreasing the friction coefficient to $\mu = 0.1$ brings the curves into even better agreement, but those simulations predict that the structure will go into macro-slip at a peak velocity of 1.0 in/s, whereas in the experiments no macro-slip was detected up to at least 2.0 in/s. For reference, the low-amplitude natural frequencies for each of the models, from which the frequency shifts were calculated, are given in Table 2.

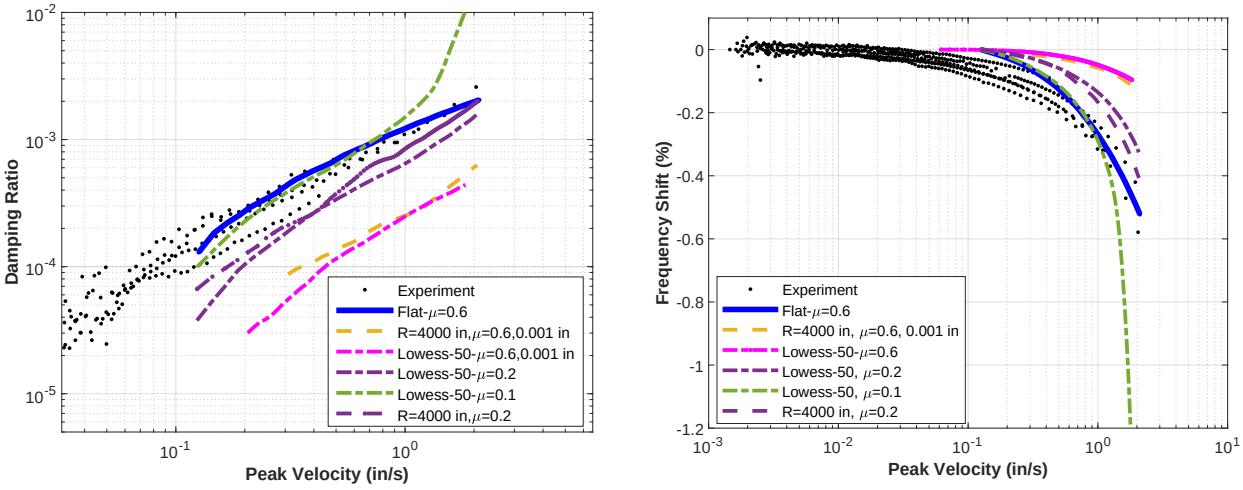

(a) Damping Ratio vs. Amplitude

(b) Frequency Shift (%) vs. Amplitude

Figure 14: Frequency and damping versus amplitude for Mode 2 at the 500 lb (2220 N) preload for friction coefficients $\mu = 0.6$, $\mu = 0.2$ and $\mu = 0.1$ for two different surface profiles.

Model	Linear Frequency (Hz)	% error
Experiment	327.77	N/A
Flat	333.12	1.63
R=4000 in, $\mu = 0.6$	328.22	0.13
R=4000 in, $\mu = 0.2$	328.14	0.11
Lowess-50, $\mu = 0.6$	327.86	0.02
Lowess-50, $\mu = 0.2$	327.78	0.00
Lowess-50, $\mu = 0.1$	327.69	−0.03

Table 2: The linear frequency values for different models in Fig. 14b for Mode 2 at the 500 lb (2220 N) preload. The third column gives the % error relative to the experimentally measured linear natural frequency.

All results thus far were for Mode 2, the first symmetric bending mode, at a 500 lb (2220 N) preload. The following section presents the experiments and predictions for Mode 6, the first torsion mode, at the same 500 lb (2220 N) preload. Subsequently, two additional sections present results for the 2000 lb (8900 N) preloads.

4.2.2. Mode 6 with 500 lb (2220 N) Preload

The experimentally measured frequency and damping for Mode 6, the first torsional mode, are compared to the QSMA predictions for various models in Fig. 15. Note that this mode exhibited much more significant nonlinearity and so that introduced additional uncertainty when seeking to extract the frequency and damping. The lower amplitude data was highly consistent and repeatable, but when impacts were performed at high levels (resulting in a frequency shift as large as 35%), there was a region in which the data became noisy. This can be see in the frequency data in Fig. 15b between 0.05 and 0.5 in/s (1.27 and 12.7 mm). In these same signals, there was clear evidence that the frequency had shifted about 35%, and so the data was retained in order to capture that fact.

In contrast with the results shown for Mode 2, the flat model and the other models with $\mu = 0.6$ all have similar damping, which is about an order of magnitude lower than the experimentally measured damping. Similarly, they all predict that the frequency should shift at much higher vibration amplitudes than it actually does. Decreasing the friction coefficient to $\mu = 0.2$ improves the agreement for both the spherical interface and Lowess smoothed models, bringing both into reasonable agreement with the measurements. Those models predict that macroslip will occur at a peak modal velocity of about 2.0 in/s (50 mm/s), which is just above the range where measurements were acquired. In the case of this mode, it did seem that macroslip may have occurred at about this amplitude level, as efforts to acquire data using higher forces showed such strong nonlinearity that the resonant peak in the spectrum completely disappeared.

The decrease in the natural frequency with amplitude is compared between the experiments and simulations in Fig. 15b. However, it is important to note that for some of the curves the simulations were not available at low enough amplitudes such that the joint would behave linearly, so there was no data from which to find the asymptote to which each curve would converge at low amplitudes. In order to address this, each frequency versus amplitude curve was

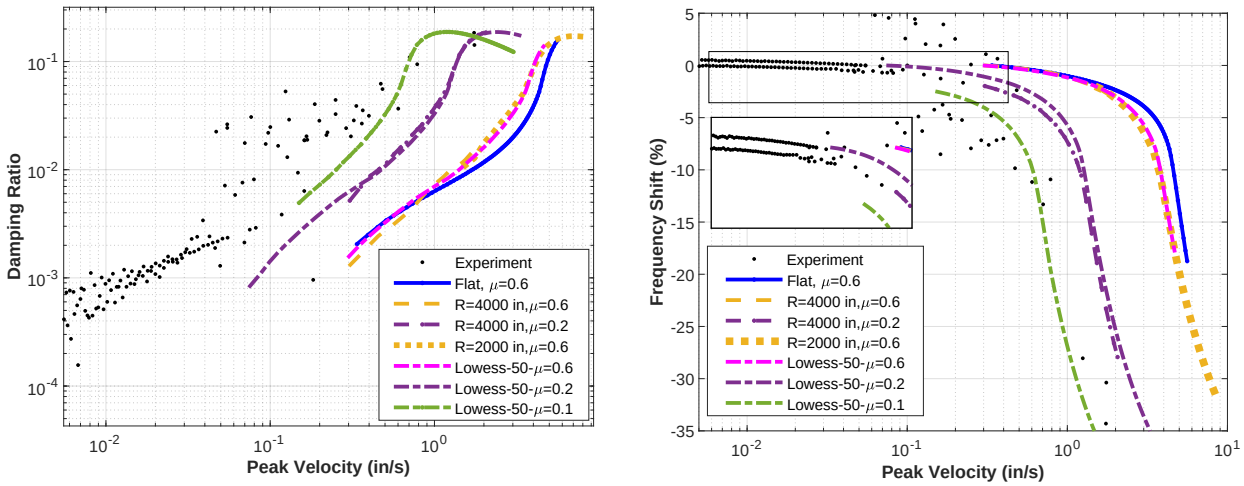

(a) Damping Ratio vs. Amplitude

(b) Frequency Shift (%) vs. Amplitude

Figure 15: Frequency and damping versus amplitude for Mode 6 (first torsion mode) at the 500 lb (2220 N) preload for friction coefficients $\mu = 0.6$, $\mu = 0.2$ and $\mu = 0.1$ for various surface profiles.

fit to a polynomial of the form $f(v) = \dfrac{1}{c_3 v^3 + c_2 v^2 + c_1 v + c_0}$, where v is the peak velocity or the horizontal axis of Fig. 18b. Then the asymptote was estimated as $f(0) = 1/c_0$ and this was subtracted from the data so all would tend toward zero at zero amplitude. The shifts required were 2.0 and 2.4 Hz for the $R = 2000$ and $R = 4000$ curves and 2.5 Hz for the Lowess-50, $mu = 0.1$ curve. In any event, one should bear in mind that, while the shape of each curve faithful to the corresponding QSMA prediction, there is some uncertainty in the vertical placement of each curve relative to the experimental results. Even then, the curves for $\mu = 0.2$ resemble the measurements both in the low-amplitude, power-law region and in capturing the large frequency shift observed at 1.0 in/s (12.7 mm).

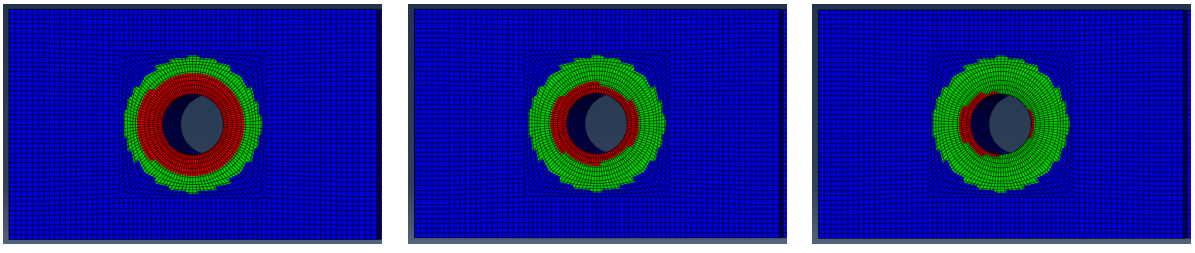

(a) Contact Status at At 0.89 in/s (23 mm/s) or 0.18 mil (4.6 μm)

(b) Contact Status at At 1.2 in/s (31 mm/s) or 0.25 mil (6.4 μm)

(c) Contact Status at At 1.4 in/s (36 mm/s) or 0.29 mil (7.4 μm)

Figure 16: Evolution of stick and slip at the contact interface for the R=4000 model with $\mu = 0.2$ when applying QSMA for Mode 6 (first torsion mode).

4.2.3. Mode 2 with 2000 lb Preload

The experimental data for Mode 2 showed considerably less nonlinearity at the 2000 lb (8900 N) preload. Even then, for each measurement the damping versus amplitude showed a clear power-law trend, and the frequency showed a clear decrease with amplitude. However, the absolute value of the damping tended to vary from one test to the next; specifically, the power-law curves shifted up and down by as much as a factor of two from one test to the next. As a result, data for several repeated trials is shown to illustrate the scatter in the data. The finite element mesh wasn't sufficient to predict the behavior of this mode to the lowest amplitudes that were measured, but one can assume that the same power-law behaviour would continue to lower amplitudes.

Comparing these results with those in Sec. 4.2.1, one observes that as the preload increased, the differences between the models became less severe. At this higher preload, changing the friction coefficient from $\mu = 0.6$ to $\mu = 0.2$ changed the damping by about a factor of two, bounding the experimental data. Once again the model with R=4000 gave very similar results to the Lowess-50 model. At this preload, the flat model over-predicts the damping, and the data fell midway between either the R=4000 or Lowess-50 models for $\mu = 0.6$ to $\mu = 0.2$. Hence, one would expect that either model would have captured the data well with $\mu \approx 0.4$. Note that the frequency curves in Fig. 17b were not shifted as was explained in the previous section, so it is left to the reader to imagine how they would compare if they had a common frequency asymptote. If such a shift was performed, then it seems that the Lowess-50 and R=4000 curves would once again correspond and would agree reasonably well with the measurements.

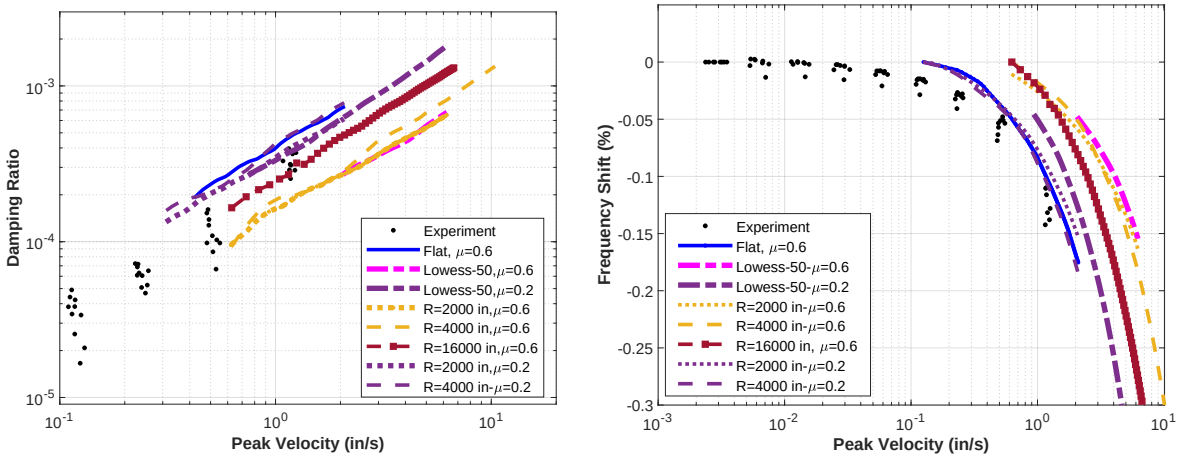

(a) Damping Ratio vs. Amplitude

(b) Frequency Shift (%) vs. Amplitude

Figure 17: Frequency and damping versus amplitude for Mode 2 at the 2000 lb (8900 N) preload for friction coefficients $\mu = 0.6$ and $\mu = 0.2$ for various surface profiles.

4.2.4. Mode 6 with 2000 lb Preload

Mode 6, the first torsion mode, showed considerable nonlinearity even when the preload was increased to 2000 lb (8900 N), as shown in Fig. 18a. The data showed a clear power-law trend for peak velocities ranging from about 0.05 to 0.5 in/s (1.2 to 12 mm/s). As was the case for this same mode at the 500 lb (2220 N) preload, the simulations that used $\mu = 0.2$ best predict the measured damping. All of the simulations predict that this mode will go into macro-slip at amplitudes that are not too much beyond those that were tested.

The decrease in the natural frequency with amplitude is compared between the experiments and simulations in Fig. 18b. As done previously for Mode 6 at 500 lb (2220 N) preload, the curves were shifted to have asyptotes near zero percent frequency error. Doing so required shifting the curves such that the low frequency asymptotes for the Flat, Lowess-50, $R = 2000$, $R = 4000$ and $R = 16000$ models were respectively 887.43, 838.9, 828.67, 849.49 and 873.49 Hz. These differ somewhat from the linearized natural frequencies computed by Abaqus's eigenvalue solver, which were reported in Sec. 4.1, and the reason for this discrepancy is not known. The frequency shift for the three models with $\mu = 0.2$ agrees best with the experimental data; the same was true for the damping curves. The model with a flat profile shows too much nonlinearity, as might be expected because its contact pressure is much less concentrated near the bolt, and so there are regions that slip more easily. The models with $\mu = 0.6$ show the correct behavior, but they predict that the system will have to reach about five times higher amplitudes to reach the same frequency shift.

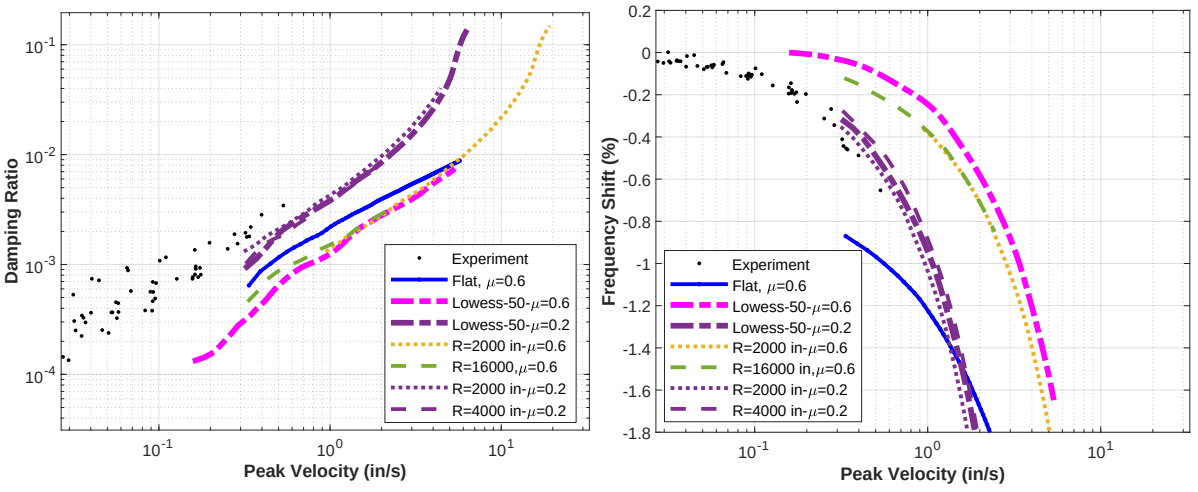

(a) Damping Ratio vs. Amplitude

(b) Frequency Shift (%) vs. Amplitude

Figure 18: Frequency and damping versus amplitude for Mode 6 (first torsion mode) at the 2000 lb (8900 N) preload for friction coefficients $\mu = 0.6$ and $\mu = 0.2$ for various surface profiles.

5. Conclusion

This work compared experimental measurements of the amplitude dependent natural frequencies and damping ratios of a simple structure called the S4 Beam in order to seek to understand the extent to which a detailed finite element model with Coulomb friction could capture the measured behavior. The only parameter tuned in the model was the Coulomb friction coefficient, and so the simulations could be considered predictive or based on first principles. To the best of the authors knowledge, this is the first study to seek to do so using finite element models with sufficient resolution that the contact behavior can be clearly observed. Other works that have sought to do similar things have used much coarser meshes, and as a result one would think that they are less predictive as each element averages over an area where the contact pressure and/or slip status varies considerably.

The contact pressure at the interface was shown to be highly sensitive to the surface topology; a curvature that causes the height to vary by only 0.15 to 0.25 mil (4 to 6 μm) over the contact interface changed the contact pressure dramatically and had a noticeable effect on how the natural frequencies varied with preload. However, various models were studied in which the surface topology was approximated to varying degrees, and in the end one could capture the relevant behavior with any model that approximated the interface geometry to a reasonable degree. It was surprising that even the damping, which depends on slip at the edges of the interface, was not very sensitive to the surface topography, even though the size and shape of the contact area changed significantly between the various models. In the end, perhaps because the damping is the net effect of all of the slip that occurs, these differences seem to be integrated out. This finding is highly encouraging, as in industrial applications it would probably be impractical to measure each contact surface as was done here.

In terms of the nonlinear behavior of the joint, which included a slight softening of the joint and a significant increase in damping with vibration amplitude, the comparisons showed that the FE model was able to match the behavior of two Modes 2 and 6 (the first symmetric bending mode and the first torsional mode, respectively), each of which stresses the interface in a very different manner. Furthermore, the behavior of these modes was well matched at two different contact pressures. This was true if the friction coefficient of the stainless steel surfaces was $\mu = 0.2$, although the uncertainty in the damping was still as much as 100% (i.e. two times too small) in some cases. Several sources report friction coefficients of around this value, so it appears that this type of model could be effective at predicting the nonlinear damping of structures such as this.

Future works should seek to extend these findings to other structures, to build more confidence in the results. It may also be interesting to see whether the finite element model can also predict coupling between the modes, as elaborated in [32]. Additionally, even though QSMA sped up the computations dramatically for this structure, the results presented here required thousands of CPU hours and in some cases the models would not converge. More efficient methods still need to be developed to make these calculations viable for industrial use. A significant fraction

of the computational expense was entailed in saving the mode shapes and mass matrix, importing those into Matlab and using them to compute the load for QSMA; the process would be much more efficient and user friendly if this were built into the native finite element code. Those operations could be readily performed in Nastran® using the DMAP feature, and this capability has begun to be implemented in the Sierra package [49] developed by Sandia National Labs.

6. Acknowledgment

This material is based in part upon work supported by the National Science Foundation under Grant Number CMMI-1561810. Any opinions,findings, and conclusions or recommendations expressed in this material are those of the author(s) and do not necessarily reflect the views of the National Science Foundation.

References

[1] C Beards. Damping in Structural Joints. *Shock Vib. Dig.*, 11(9):35–41, 1979.

[2] D Dini and D Nowell. Prediction of the slip zone friction coefficient in flat and rounded contact. *Wear*, 254(3-4):364–369, 2003.

[3] Christian M Firrone, Stefano Zucca, and Muzio M Gola. The effect of underplatform dampers on the forced response of bladed disks by a coupled static/dynamic harmonic balance method. *Int. J. Non. Linear. Mech.*, 46(2):363–375, 2011.

[4] Xiangqing W Tangpong, Jonathan A Wickert, and Adnan Akay. Distributed friction damping of traveling wave vibration in rods. In *Int. Des. Eng. Tech. Conf. Comput. Inf. Eng. Conf.*, volume 48027, pages 1339–1348, 2007.

[5] J Esteban and C A Rogers. Energy dissipation through joints: Theory and experiments. *Comput. Struct.*, 75(4):347–359, 2000.

[6] D D Quinn and D J Segalman. Using series-series Iwan-type models for understanding joint dynamics. *J. Appl. Mech. Trans. ASME*, 72(5):666–673, 2005.

[7] C W Schwingshackl, E P Petrov, and D J Ewins. Measured and estimated friction interface parameters in a nonlinear dynamic analysis. *Mech. Syst. Signal Process.*, 28:574–584, 2012.

[8] Matthew R W Brake. *The Mechanics of Jointed Structures: Recent Research and Open Challenges for Developing Predictive Models for Structural Dynamics*. Springer, 1st edition, 2018.

[9] Bharat Bhushan. *Concepts and Applications of Tribology*. Wiley, 2nd edition, 2013.

[10] A A Ferri. Friction damping and isolation systems. *J. Mech. Des. Trans. ASME*, 117(B):196–206, 1995.

[11] R A Ibrahim and C L Pettit. Uncertainties and dynamic problems of bolted joints and other fasteners. *J. Sound Vib.*, 279(3-5):857–936, 2005.

[12] D J Segalman, D L Gregory, M J Starr, B R Resor, M D Jew, J P Lauffer, and N M Ames. Handbook on Dynamics of Jointed Structures. Technical Report SAND2009-4164, Sandia National Laboratories, Albuquerque, New Mexico, 2009.

[13] L Gaul and J Lenz. Nonlinear dynamics of structures assembled by bolted joints. *Acta Mech.*, 125(1-4):169–181, 1997.

[14] Daniel Joseph Segalman. A modal approach to modeling spatially distributed vibration energy dissipation. Technical Report SAND2010-4763, 993326, aug 2010.

[15] C F Beards. Damping in Structural Joints Shock and Vibration Digest. *Shock and Vibration Digest*, 21(4):3 – 5, 1989.

[16] E E Ungar. The status of engineering knowledge concerning the damping of built-up structures. *J. Sound Vib.*, 26(1):141–154, jan 1973.

[17] L Gaul and R Nitsche. The role of friction in mechanical joints. *Appl. Mech. Rev.*, 54(2):93–106, 2001.

[18] Xinglin Lei. How do asperities fracture? An experimental study of unbroken asperities. *Earth Planet. Sci. Lett.*, 213(3-4):347–359, 2003.

[19] A Fantetti, L R Tamatam, M Volvert, I Lawal, L Liu, L Salles, M R W Brake, C W Schwingshackl, and D Nowell. The impact of fretting wear on structural dynamics: Experiment and Simulation. *Tribol. Int.*, 138:111–124, 2019.

[20] Hamid Ghaednia, Xianzhang Wang, Swarna Saha, Yang Xu, Aman Sharma, and Robert L Jackson. A review of elastic–plastic contact mechanics. *Appl. Mech. Rev.*, 69(6), 2017.

[21] E J Berger. Friction modeling for dynamic system simulation. *Appl. Mech. Rev.*, 55(6):535–577, 2002.

[22] H Festjens, G Chevallier, and J L Dion. Nonlinear model order reduction of jointed structures for dynamic analysis. *J. Sound Vib.*, 333(7):2100–2113, 2014.

[23] Matthew S Allen, Robert Lacayo, and Matthew R W Brake. Quasi-static Modal Analysis based on Implicit Condensation for Structures with Nonlinear Joints. sep 2016.

[24] Robert M Lacayo and Matthew S Allen. Updating Structural Models Containing Nonlinear Iwan Joints Using Quasi-Static Modal Analysis. *Mech. Syst. Signal Process.*, Volume 118(1 March 2019):133–157, 2019.

[25] Aabhas Singh, Mitchell Wall, Matthew S Allen, and Robert J Kuether. Spider Configurations for Models with Discrete Iwan Elements. In

Nonlinear Struct. Syst. Vol. 1, pages 25–38. Springer, 2020.

[26] David A Najera-Flores and Robert J Kuether. A study of whole joint model calibration using quasi-static modal analysis. *Journal of Vibration and Acoustics*, 142(5), 2020.

[27] Nidish Narayanaa Balaji and Matthew R W Brake. A quasi-static non-linear modal analysis procedure extending Rayleigh quotient stationarity for non-conservative dynamical systems. *Comput. & Struct.*, 230:106184, 2020.

[28] Matthew S. Allen, Joseph D. Schoneman, Wesley Scott, and Joel W. Sills. Application of Quasi-Static Modal Analysis to an Orion Multi-Purpose Crew Vehicle Test. In *38th International Modal Analysis Conference (IMAC XXXVIII)*, Houston, Texas, February 2020.

[29] Emily Jewell, Matthew S Allen, Iman Zare, and Mitchell Wall. Application of quasi-static modal analysis to a finite element model and experimental correlation. *J. Sound Vib.*, 479:115376, 2020.

[30] Aabhas Singh, Matteo Scapolan, Yuta Saito, Matthew S Allen, Daniel Roettgen, Ben Pacini, and Robert J Kuether. Experimental Characterization of a New Benchmark Structure for Prediction of Damping Nonlinearity. In *Nonlinear Dynamics, Volume 1*, pages 57–78. Springer International Publishing, Cham, 2018.

[31] Adam R Brink, Robert J Kuether, Matthew D Fronk, Bryan L Witt, and Brendan L Nation. Contact stress and linearized modal predictions of as-built preloaded assembly. *Journal of Vibration and Acoustics*, 142(5):051106, 2020.

[32] Mitchell Wall, Matthew S. Allen, and Robert J. Kuether. Observations of modal coupling due to bolted joints in an experimental benchmark structure. *Mechanical Systems and Signal Processing*, 162:107968, 2022.

[33] Iman Zare and Matt Allen. Adapting a Contact-Mechanics Algorithm to Predict Damping in Bolted Joints using Quasi-Static Modal Analysis. *Int. J. Mech. Sci.*, 189:105982, 2020.

[34] Mitchell Wall, Matthew S Allen, and Iman Zare. Predicting S4 Beam Joint Nonlinearity Using Quasi-Static Modal Analysis. In *Nonlinear Struct. Syst. Vol. 1*, pages 39–51. Springer, 2020.

[35] FEA Abaqus et al. Dassault systemes simulia corporation. *Providence, Rhode Island, USA*, 2021.

[36] Xi Shi and Andreas A Polycarpou. Measurement and modeling of normal contact stiffness and contact damping at the meso scale. *J. Vib. Acoust.*, 127(1):52–60, 2005.

[37] Andreas A. Polycarpou and Izhak Etsion. Analytical Approximations in Modeling Contacting Rough Surfaces. *Journal of Tribology*, 121(2):234–239, 04 1999.

[38] William S. Cleveland, Susan J. Devlin, and Eric Grosse. Regression by local fitting: Methods, properties, and computational algorithms. *Journal of Econometrics*, 37(1):87–114, 1988.

[39] Rizal Isnanto. Comparation on several smoothing methods in nonparametric regression. *Jurnal Sistem Komputer*, 1(1):41–48, 2011.

[40] Matthew S Allen and Jerry H Ginsberg. A Global, Single-Input-Multi-Output (SIMO) Implementation of The Algorithm of Mode Isolation and Applications to Analytical and Experimental Data. *Mech. Syst. Signal Process.*, 20:1090–1111, 2006.

[41] Michael Feldman. Non-linear system vibration analysis using hilbert transform–ii. forced vibration analysis method'forcevib'. *Mechanical Systems and Signal Processing*, 8(3):309–318, 1994.

[42] Brandon J. Deaner, Matthew S. Allen, Michael J. Starr, Daniel J. Segalman, and Hartono Sumali. Application of viscous and iwan modal damping models to experimental measurements from bolted structures. *J. Vib. Acoust. Trans. ASME*, 137(2):12, 2015.

[43] K L Johnson. *Contact Mechanics*. Cambridge University Press, Cambridge, United Kingdom, 4th edition, 1985.

[44] Robert M Lacayo, Brandon J Deaner, and Matthew S Allen. A numerical study on the limitations of modal Iwan models for impulsive excitations. *J. Sound Vib.*, 390:118–140, mar 2017.

[45] Daniel J Segalman. A Four-Parameter Iwan Model for Lap-Type Joints. *J. Appl. Mech.*, 72(5):752–760, sep 2005.

[46] T. Dreher, M.R.W. Brake, B. Seeger, and M. Krack. In situ, real-time measurements of contact pressure internal to jointed interfaces during dynamic excitation of an assembled structure. *Mechanical Systems and Signal Processing*, 160:107859, 2021.

[47] Nicholas Karpov, Justin Porter, and Matthew R.W. Brake. Masing manifolds: Reconciling the masing conditions with real hysteresis. In *40th International Modal Analysis Conference (IMACXL)*, 2022.

[48] A Fantetti, C Pennisi, D Botto, S Zucca, and C Schwingshackl. Comparison of contact parameters measured with two different friction rigs for nonlinear dynamic analysis. In *International Conference on Noise and Vibration Engineering*, volume 730, 2020.

[49] David A. Najera-Flores and Robert J. Kuether. A Study of Whole Joint Model Calibration Using Quasi-Static Modal Analysis. *Journal of Vibration and Acoustics*, 142(5), 06 2020. 051109.